Journal of Hazardous Materials 460 (2023) 132494

Contents lists available at ScienceDirect

Journal of Hazardous Materials

journal homepage: www.elsevier.com/locate/jhazmat

Research Paper

Fast pyrolysis kinetics of waste tires and its products studied by a wireless-powered thermo-balance

Boyu Qu [a], Chuanqun Liu [a], Yinxiang Wang [a], Aimin Li [a], Yi Qu [a], Ye Shui Zhang [b,*], Guozhao Ji [a,*]

[a] Key Laboratory of Industrial Ecology and Environmental Engineering, School of Environmental Science & Technology, Dalian University of Technology, Dalian 116024, China

[b] School of Engineering, University of Aberdeen, Aberdeen AB24 3UE, UK

HIGHLIGHTS

- A novel thermal balance with wireless power enabled the in-situ mass measurement.
- Kinetics of waste tire fast pyrolysis was analyzed to overcome the TGA limitation.
- The extremely increased heating rate reduced the apparent activation energy.
- High heating rates greatly reduced the occurrence of secondary reactions.
- High heating rates favored the release of trimer isoprene from waste tire.

GRAPHICAL ABSTRACT

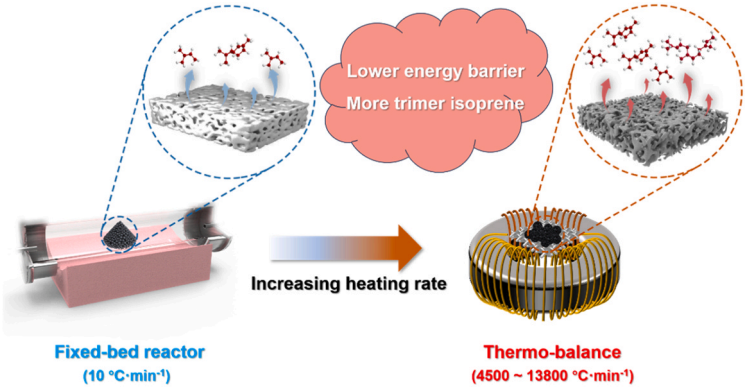

ARTICLE INFO

Editor: Feng Xiao

Keywords:
Fast pyrolysis
Kinetics
Waste tires
in-situ weight measurement
Wire mesh

ABSTRACT

Fast pyrolysis is commonly used in industrial reactors to convert waste tires into fine chemicals and fuels. However, current thermogravimetric analyzers are facing limitations that prevent the acquisition of kinetic information. To better understand the reaction kinetics, we designed a novel thermo-balance device that was capable of in-situ weight measurement during rapid heating. The results showed that the reaction rate substantially increased, with significant reductions in reaction time and apparent activation energy compared to slow pyrolysis. The change of reaction mechanism from the reaction order model to the nucleation and growth model was responsible for the increase in the degradation rate. Fast pyrolysis led to the generation of more trimers of isoprene as primary pyrolytic volatiles, which we further supported through density functional theory calculations. The findings suggested that fast pyrolysis has a higher chance of overcoming the high energy barrier to form trimers of isoprene. This comprehensive and in-depth understanding of fast pyrolysis kinetics and product distribution could reveal a more realistic process of waste pyrolysis, which benefited the industry.

* Corresponding authors.
E-mail addresses: yeshui.zhang@abdn.ac.uk (Y.S. Zhang), guozhaoji@dlut.edu.cn (G. Ji).

https://doi.org/10.1016/j.jhazmat.2023.132494
Received 19 May 2023; Received in revised form 28 August 2023; Accepted 4 September 2023
Available online 8 September 2023

1. Introduction

Since the 21st century, with the explosive growth of the population and economy, the number of vehicles has been growing continuously worldwide [1]. A study surveyed 51 nations encompassing 90% of vehicles all around the world, stating that there were approximately 26 million tons of waste tires (WTs) coming to the end [2]. What is worse is that WTs are non-biodegradable [2] and adversely affect the ecosystem [3]. Hence, there is a need to develop an environment-friendly technique to tackle the associated environmental concerns caused by the massive amount of WTs. Various thermo-conversion techniques [4–6] have been adopted to convert WTs into valuable products. Therein, pyrolysis [7–9] is regarded as one of the most promising technologies as there are less hazardous gas emissions (e.g., CO and SO_2) and more high calorific value gaseous products (e.g., H_2 and CH_4) due to the absence of oxygen [10]. Also, pyrolytic oil consists of various high-value chemical products [11], and pyrolytic char can be used to produce carbon nanomaterials[12] and electrodes [13]. Thus, pyrolysis has raised extensive research attention by many researchers.

Due to the simple design, the fixed-bed reactor has been widely used for waste tire pyrolysis. However, poor heat transfer in the fixed-bed reactor combined with the batch operating mode often requires long residence time and iterative cooling/heating. To address these issues, alternative reactors have been investigated, such as fluidized-bed and molten-bed reactors, which allow for high heating rates and continuous feeding. Nevertheless, the thermal history of feedstock in the fixed-bed and fluidized-bed behaved very differently. A study [14] reported that at the same pyrolysis temperature, the raised heating rate could decrease the gas and char yields but increase the oil yield. Even at the high temperature of 1000 °C, high oil yield could still be observed which was opposite to what was observed at a low heating rate. As discussed above, fast and slow pyrolysis could lead to very different pyrolysis processes and significantly impact product yields. Therefore, an in-depth study on WTs fast pyrolysis at high heating rates is necessary to gain a deeper understanding of the reaction mechanism and provide valuable insights for the industry.

Thermal kinetic analysis is an effective method to investigate and simulate the thermal degradation process of solid organic wastes. The kinetic analysis using the data obtained by a thermogravimetric (TG) analyzer could be critical for the design of industrial reactors. Previous studies [15–17] focused on the pyrolysis kinetics at low heating rates (<1000 °C min^{-1}) with few studies reporting the kinetics of waste pyrolysis at high heating rates. Exploring pyrolysis kinetics at high heating rates (>1000 °C min^{-1}) is essential for two main reasons. Firstly, high heating rates can induce significantly differing pyrolysis behaviors. Secondly, reaction rate, heat, and mass transfer interact with each other in fluidized-bed reactor simulations, and inadequate kinetics may result in inaccurate computational fluid dynamics (CFD) model predictions. Thus, an in-depth study of the pyrolysis kinetics of wastes at high heating rates is necessary, both for the enhanced understanding of the process and for accurate reactor design and modeling. Commercial TG analyzers are limited to achieving a heating rate of only 1000 °C min^{-1} at most, such as the STA 449 F1 Jupiter, which is much slower than the heating rates required in fast pyrolysis experiments. To overcome this limitation, Zhang et al. [18] designed and employed a self-made wire--mesh reactor with a liquid nitrogen cooling unit to achieve *ex-situ* mass measurement after the sample temperature dropped to − 196 °C. However, this technique had some limitations in terms of the accuracy and reproducibility of mass measurements, as well as insufficient data points, which in turn limited the kinetic analysis of the reaction. Therefore, in-situ mass measurement methods such as TG analysis with a much higher heating rate are crucial in investigating the behavior of fast pyrolysis.

With the use of our designed wire mesh reactor employing in-situ TG measurement, we were able to establish the kinetics of fast pyrolysis. Additionally, an updated cracking mechanism of WTs polymer was proposed based on both experimental investigations and theoretical calculations. The kinetic and product distribution studies conducted thoroughly the differences between fast and slow pyrolysis of WTs, which could provide valuable guidance to industries in designing large-scale reactors for WTs pyrolysis.

2. Materials and methods

2.1. Materials

To minimize the effect of heat transfer, the WTs powder was sieved by a 200-mesh screen to keep the particle diameter less than 0.075 mm. The proximate analysis and ultimate analysis of WTs were reported in our previous study [19].

2.2. Pyrolysis experiments

The schematic diagrams of the novel thermo-balance device and wire mesh reactor are depicted in Fig. 1. The physical diagrams are shown in Fig. S1.

The novel thermo-balance device consisted of a mass acquisition unit, a wire mesh heating system, and an infrared (IR) temperature measurement module. The mass acquisition unit was composed of a precision electronic balance with an accuracy of 0.01 mg and a mass data collection module with a collection frequency of 50 Hz. This allowed for real-time mass acquisition during heating. In the heating system, the sample was placed on a wire mesh and could be heated at a considerably high heating rate due to the small heat capacity of the wire mesh. Both ends of the wire mesh were connected to the secondary coil (the blue part of 3 as shown in Fig. 1a) which was powered wirelessly via the electromagnetic coil, allowing for the mass variation recording without interference from cables. The IR temperature measurement module consisted of a commercial IR thermometer with an accuracy of 0.1 °C and a temperature recording module with a recording frequency of 1000 Hz. After the calibration, the device was capable of in-situ weight measurement at high heating rates (>500 °C min^{-1}). The parameters of each experiment are listed in Table S1.

A wire mesh reactor was constructed with a tar trap (Fig. 1b) filled with silica wool as a heat transfer medium. Liquid nitrogen was used as an efficient cooling agent in the space between the inner and outer tubes. To maintain consistent thermal conditions, a wire mesh with the same size and current was used.

The WTs pyrolysis experiments at low heating rates were also conducted using a commercial TG analyzer (Netzsch STA2500) and a fixed-

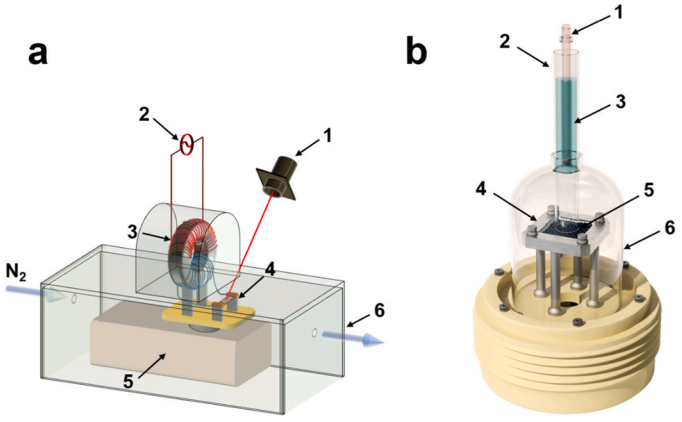

Fig. 1. The schematic diagrams of the novel thermo-balance device and wire mesh reactor. a Thermobalance device. 1-Infrared thermometer; 2-AC power; 3-Electromagnetic coil; 4-Wire mesh; 5-Analytical balance; 6-Plexiglass shell. b Wire mesh reactor. 1-Gas outlet; 2-Oil trap; 3-Liquid nitrogen; 4- Power supply; 5-Wire mesh; 6-Quartz glass shell.

bed reactor. All experiments were reduplicated three times to ensure the reproducibility of results. Details of the experimental conditions can be found in the Supplemental Information (SI) file.

2.3. Products analysis

The yields of solid, gas, and liquid products were defined by Eq. (1~3).

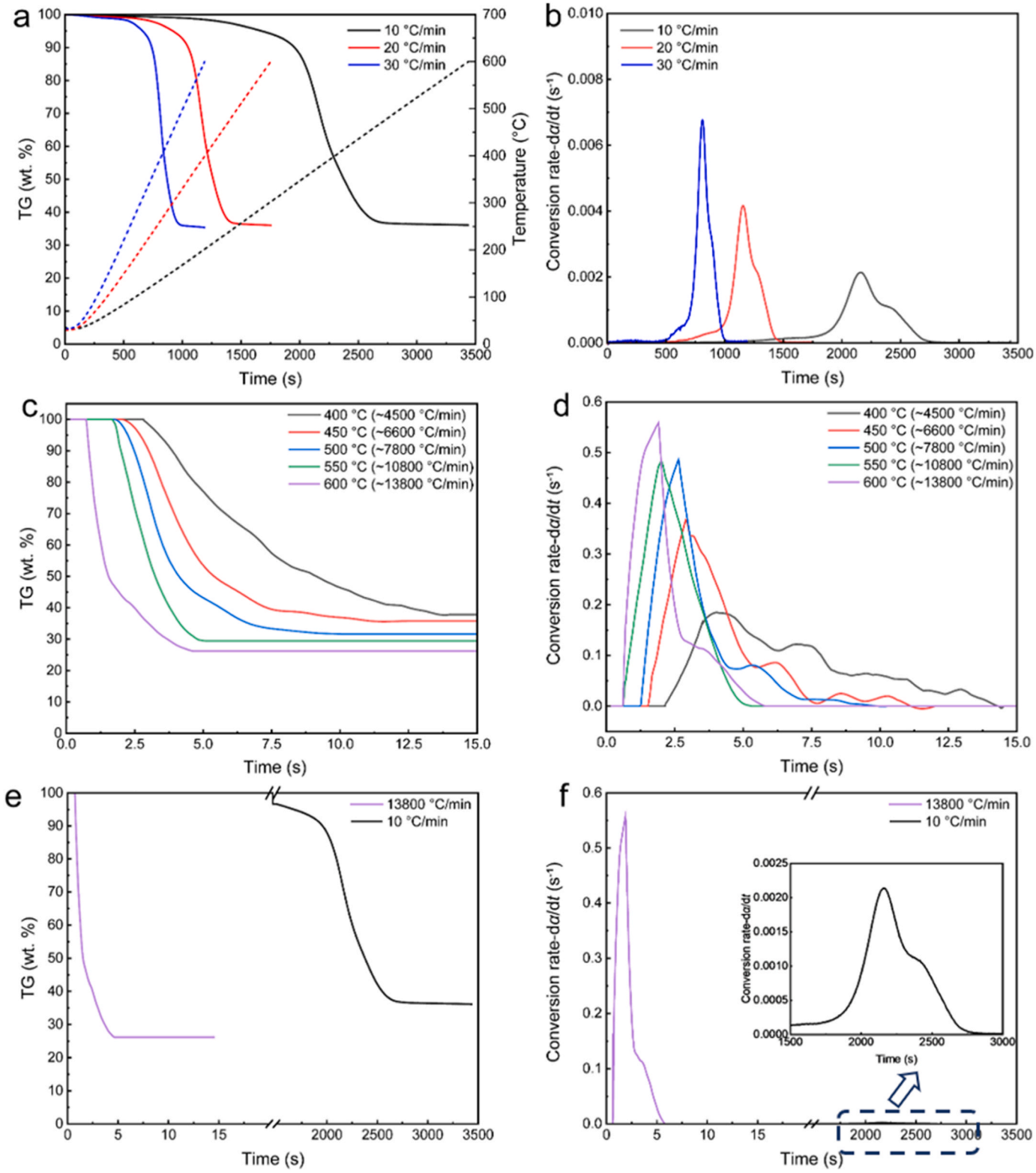

Fig. 2. TG data obtained from fast and slow pyrolysis. a TG and b conversion rate curves of WT slow pyrolysis. c TG and d conversion rate curves of WT fast pyrolysis. e TG and f conversion rate curves with the same temperature of 600 °C in fast and slow pyrolysis.

$$Y_{Solid} = \frac{m_{Solid}}{m_{Feedstock}} \times 100\% \quad (1)$$

$$Y_{Gas} = \frac{m_{Gas}}{m_{Feedstock}} \times 100\% \quad (2)$$

$$Y_{Oil} = 100\% - Y_{Soild} - Y_{Gas} \quad (3)$$

where, Y_{Solid}, Y_{Gas}, and Y_{Oil} represented the yield of solid, gas, and liquid products, and m_{Solid} and m_{Gas} were the mass of solid and gas products. The methods to compute m_{Solid} and m_{Gas} are detailed in the Supplementary Information.

The pyrolysis products were characterized by a Micro Gas Chromatography (GC), Gas Chromatography-Mass Spectrometry Analyzer (GC/MS), in-situ Pyrolysis Electron Ionization/Vacuum Ultraviolet Photoionization Time-of-Flight Mass Spectrometer (Py-EI/VUVPI-TOF-MS), Elemental Analyzer, Fourier Transform Infrared Spectrometer (FTIR), N_2 Physi-sorption analyzer, Scanning Electron Microscope (SEM) and Raman Spectrometer (Raman). Further details about the characterization can be found in the Supplementary Information.

2.4. Kinetic method

The kinetics study is to parameterize the process rate as a function of state variables (e.g., reaction time t, reaction conversion α, and the temperature T), so that it can predict any combination of these variables and provide insights into the reaction mechanisms. Arrhenius empirical equation was employed to describe the thermally stimulated process [20].

$$\frac{d\alpha}{dt} = A\exp\left(\frac{-E}{RT}\right)f(\alpha) \quad (4)$$

E was the apparent activation energy. For a complex reaction (polymer thermal degradation), it was discovered that there was a dependence between the conversion and apparent activation energy. To obtain this dependence, the temperature dependence of the isoconversional rate was needed by performing a series of runs at different temperature programs. Thus, E could be obtained by the mathematical calculation (The detailed derivation is shown in the SI).

$$E_\alpha = -\frac{[\partial \ln(d\alpha/dt)]}{\partial[(RT)^{-1}]} \quad (5)$$

Pre-exponential factor A and reaction model $f(\alpha)$ can be obtained by compensation effect [20,21]. On the macro level, the value of reaction model $f(\alpha)$ denoted the driving force of the reaction and its expression depended on the reaction mechanism.

3. Results and discussions

3.1. TG analysis of WTs fast and slow pyrolysis

The profile of WTs slow pyrolysis was studied using a TG analyzer. Fig. 2a-b present TG and conversion rate curves at three different heating rates of 10, 20, and 30 °C min^{-1}, respectively. As shown in Fig. 2a, the temperature range corresponding to the main decomposition process was from 200° to 500°C with a residual mass fraction of approximately 36%, consisting primarily of pyrolytic char and ash. This observation was consistent with the results of our reported proximate analysis of WT samples [19]. A total weight loss of 55.4% was observed in this stage within the temperature range between 300 and 450 °C. The mass fraction of volatile matter from the reported proximate analysis was 63.3%, and almost 87.5% of the volatile was produced from this stage. This could be ascribed to the thermal decomposition of natural rubber (NR) and butyl rubber (BR) [22]. The finding could also be supported by the primary peak and followed by a shoulder peak as shown in Fig. 2b. It was commonly recognized that the primary peak corresponds to the decomposition of NR with the corresponding temperature range of 300–410 °C [23]. The following shoulder peak is corresponding to the decomposition of BR at the temperature between 410 and 450 °C [24].

To investigate the WTs fast pyrolysis behaviors, WT samples were heated from room temperature to target temperatures (400, 450, 500, 550, and 600 °C) at different high heating rates (~4500, ~6600, ~7800, ~10,800, and ~13,800 °C min^{-1}). Moreover, a comparison of TG data obtained from various fast pyrolysis experiments was performed, and reaction time t was employed as an independent variable in the curves of TG and conversion rate.

Fig. S2 depicts the curves of TG and temperature with different respective target temperatures (400, 450, 500, 550, and 600 °C) and different heating rates (~4500, ~6600, ~7800, ~10,800, and ~13,800 °C min^{-1}). Obviously, there were non-isothermal pyrolysis stage (stage I) and isothermal pyrolysis stage (stage II) in the thermal degradation process. According to the above analysis of WTs slow pyrolysis, the whole thermal degradation process intensively occurred in a temperature range between 200 and 500 °C. Thus, at 400 and 450 °C, minor weight loss occurred during the isothermal pyrolysis stage. The most of volatiles were released from the solid phase reaction region in the isothermal pyrolysis stage. However, an opposite trend was found that major thermal decomposition happened in the non-isothermal pyrolysis stage at 500, 550, and 600 °C. As presented in Fig. 2c, with the increase in heating rate, the mass fraction of the residual decreased from 37.6% at 400 °C to 26.2% at 600 °C which indicated that the increase in heating rate promoted the pyrolysis of WTs to produce more non-solid products. In Fig. 2d, the variation of the conversion rate curve was minor and spanned a wide time range at 400 °C. By contrast, the main weight loss peak shifted to the lower temperature with the increased heating rate, which suggested a higher heating rate could trigger an earlier initiation of the pyrolysis reaction.

To better illustrate the difference between the slow and fast pyrolysis behaviors, the TG and conversion rate curves of pyrolysis at a target temperature of 600 °C were compared under two conditions, as shown in Fig. 2e-f. A significant increase in heating rate resulted in a sharp reduction in reaction time by 2–3 orders of magnitude (~2750 s → ~5 s) indicating that the heating rate played a decisive role in changing WTs pyrolysis behaviors. The mass fraction of pyrolysis residual was decreased from ~36% to ~26.2% while the heating rate was increased from 10 to ~13,800 °C min^{-1}. From Fig. 2f, compared with the reaction rate curve of slow pyrolysis, the shape of fast pyrolysis $d\alpha/dt$ was narrower and sharper, which indicated WTs fast pyrolysis needed less reaction time and proceeded much faster. Also, a primary weight loss peak and a shoulder peak were still evident, which indicated there was a clear boundary between the pyrolysis of NR and BR regardless of heating rates.

3.2. Comparison of apparent activation energies of fast and slow pyrolysis

The apparent activation energies of the WTs fast and slow pyrolysis processes were determined from the Arrhenius plots of Friedman's differential iso-conversional method [25], as shown in Fig. 3a. The apparent activation energy distributions for both fast and slow pyrolysis processes varied with the increase in conversion, suggesting that WTs pyrolysis involved complex and competitive chemical reactions. The apparent activation energy range for WTs slow pyrolysis increased from 119 to 306 kJ mol^{-1}. The lower apparent activation energy at the conversion stage of 0.05–0.10 was caused by the decomposition of limited light volatile organic matter with low-boiling points. In the conversion stage of 0.1–0.6, which was dominated by the thermal decomposition of NR, the variation range of apparent activation energy was about 220–230 kJ mol^{-1}. In this stage, the apparent activation energy was relatively stable at ~225 kJ mol^{-1}, consistent with Seidelt's study [24]. In the stage corresponding to 0.75–0.95, the thermal degradation of BR occurred, and the apparent activation energy was almost constant

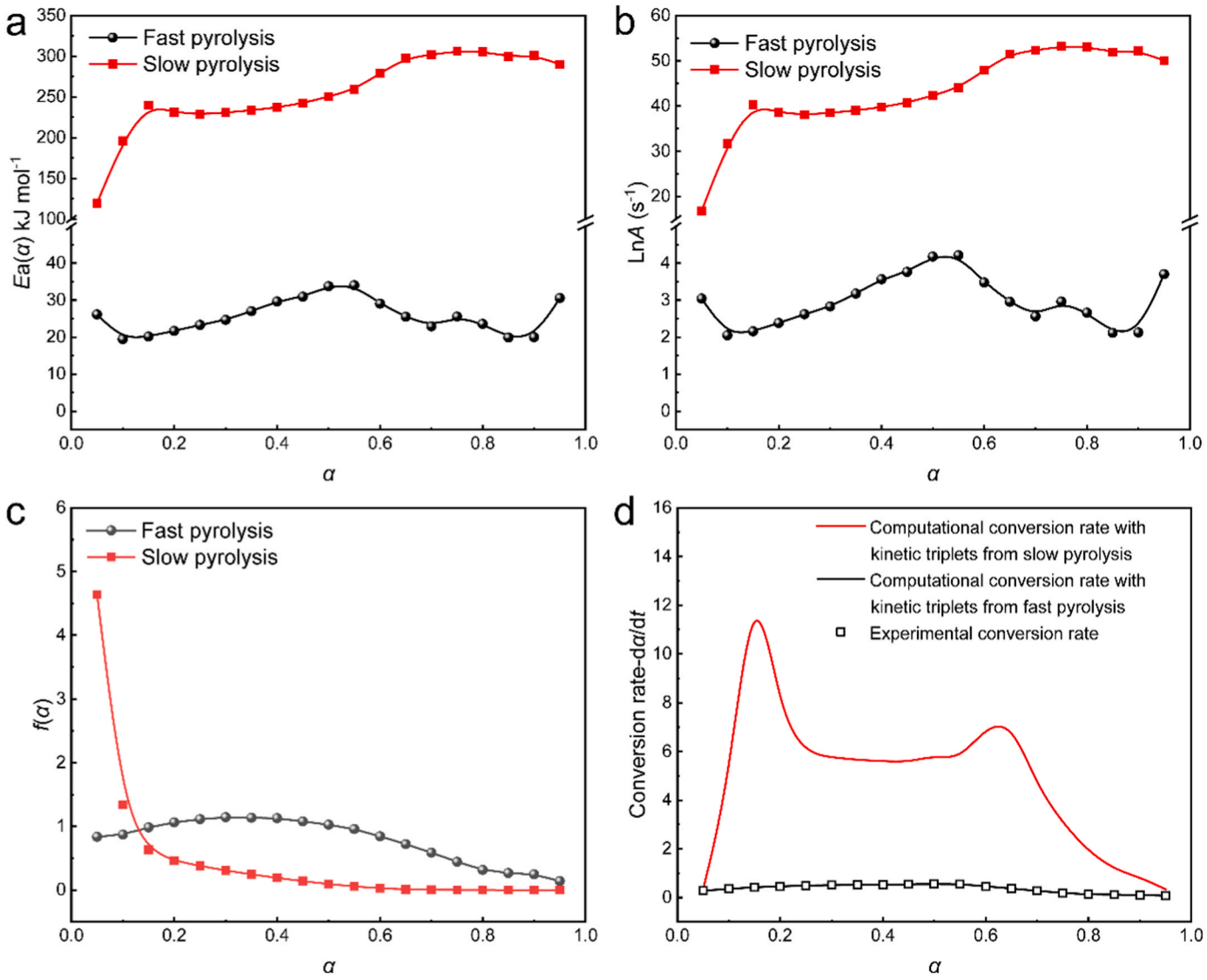

Fig. 3. Kinetics and model evaluation for fast and slow pyrolysis. a The apparent activation energy distribution. b The logarithm of pre-exponential factors and c computed reaction models of WT fast and slow pyrolysis. d The comparison of the computational conversion rate which calculated WT fast pyrolysis process based on kinetics parameters of fast and slow pyrolysis and experimental conversion rate.

(~284 kJ mol^{-1}). The difference in apparent activation energies indicated that BR has more stable complex chemical structures compared with NR [26].

For fast pyrolysis, there was a significant drop in the apparent activation energy of the entire WTs pyrolysis process. In Fig. 3a, an increased apparent activation energy followed by a decrease with conversion was observed. In general, the pyrolysis apparent activation energy of NR was close to BR. In the NR pyrolysis stage ($0.1 < \alpha < 0.6$), unlike the variation trend of apparent activation energy for WTs slow pyrolysis, WTs fast pyrolysis showed an increasing trend followed by a decreasing trend.

Thermal degradation kinetics was indispensable for the design and optimization of industrial reactors. Pyrolysis kinetics defined the required conditions for thermal decomposition to occur and provided information on the reaction rate and time requirement to complete the thermal degradation. The reaction model was a theoretical function that reflected the process of pyrolysis. Thus, in order to obtain the complete reaction kinetics, apparent activation energy, reaction models, and pre-exponential factors were indispensable.

Based on the solid reaction physical models listed in Table S2, 15 pairs of activation energies and logarithms of pre-exponential factors were calculated to derive the compensation line and the reaction model [25]. According to the characteristics of the compensation effect between activation energies and pre-exponential factors, 15 pairs of E and ln$A$ were fitted on a straight compensation line as shown in Fig. S3. The equation of the compensation line for WTs slow pyrolysis was:

$$\ln A_\alpha = 0.1948E_\alpha - 6.4748 \quad (6)$$

and for WTs fast pyrolysis was:

$$\ln A_\alpha = 0.149E_\alpha - 0.8497 \quad (7)$$

The reaction models of WTs fast and slow pyrolysis were presented in Fig. 3c. In slow pyrolysis, the overall trend of the $f(\alpha)$ curve was a monotonical decrement. The rapid decrease of $f(\alpha)$ in the initial stage ($0.05 < \alpha < 0.1$) of slow pyrolysis was consistent with the 2D diffusion model (D_2) curve at a low conversion range, corresponding to the elimination of moisture and light volatile organic matter with low-boiling points. In this stage, less volatiles were generated and released from the solid phase. There was almost no obvious pore structure in the residue. Thus, the mass transfer of volatiles from solid phases might be the limiting step of WTs in this stage. After that, NR and BR acted as the

main reactants with large amounts of hydrocarbon production and a notable decrement in the solid mass fraction. As the previous diffusion-limiting step did not form sufficient voids for the hydrocarbon diffusion, some hydrocarbons still had the possibility to be trapped in the solid. This part of the volatile had been collected as oil, but eventually altered to solid products. It took a while to form sufficient voids. Once the diffusion rate was high enough, the limiting step was no longer diffusion. During the processes of NR and BR pyrolysis, the reaction mechanism could be described by an order-based model with an order between 2 and 3. A noteworthy aspect of the reaction order model is that the reaction rate is proportional to the remaining concentration of the reactants. This implied that the overall trend of the pyrolysis rate decreased as the reaction proceeds, due to the reduction in the concentration of reactants [27].

As depicted in Fig. 3c, a clear distinction in the $f(\alpha)$ values was observed between fast and slow pyrolysis. Unlike slow pyrolysis, fast pyrolysis exhibited increased $f(\alpha)$ values followed by a decrease in conversion. These results highlighted the dominant role of exceptional heating rates in the pyrolysis process of WTs. In the stage of NR decomposition ($0.1 < \alpha < 0.6$), the kinetic model was altered from the reaction order model (F_{2-3}) to the random nucleation and nuclei growth model (A_2). Due to the high heating rate, the upcoming degradation reaction was triggered in a high-temperature environment, and volatiles were released abruptly to form a structure with pores which proved the limiting step was no longer diffusion. Moreover, due to the high-temperature environment, the degradation was accompanied by the generation of solid chars. It indicated the kinetic model was changed into A_2 which could be regarded as a transformation from rubber to char via nucleation and nuclei growth.

According to the nucleation and nuclei growth model, the WTs pyrolysis could be regarded as a transformation from rubber to char. During fast pyrolysis, new nuclei quickly formed due to the rapid release of volatiles from the solid phase, which could act as nucleation seeds for the further formation of char. The increment in the nucleus size and the nuclei number led to a higher char formation rate. This nucleation and growth process was supported by the increased reaction rate. Since the energy barrier of nucleus growth was generally lower than that of nucleus generation, this could explain why the apparent activation energy increased at the beginning.

Fig. S4 depicts the comparison of the predicted conversion obtained by kinetic parameters and the corresponding experimental conversions of slow pyrolysis. The comparison of fast pyrolysis conversions predicted by the kinetic model and experimental conversion data at different final temperatures is shown in Fig. S5. However, if the slow pyrolysis kinetic parameters were used to fit the fast pyrolysis experimental conversions, the kinetic model would fail.

As demonstrated in Fig. 3d, there was a huge difference between the conversion rates calculated from slow pyrolysis kinetic parameters and those measured from fast pyrolysis. But the kinetic parameters derived from our mesh-wire reactor could accurately predict both conversions (Fig. S5) and conversion rate (Fig. 3d) during the fast pyrolysis process. This finding suggested that using kinetic parameters derived from commercial TG analyzers to represent fast pyrolysis is inappropriate. This was because the extremely different thermal history could alter the pyrolysis mechanism in terms of apparent activation energy, pre-exponential factor, and reaction models.

3.3. WTs fast and slow pyrolysis characteristics

The distributions of gas, liquid, and char from WTs pyrolysis at

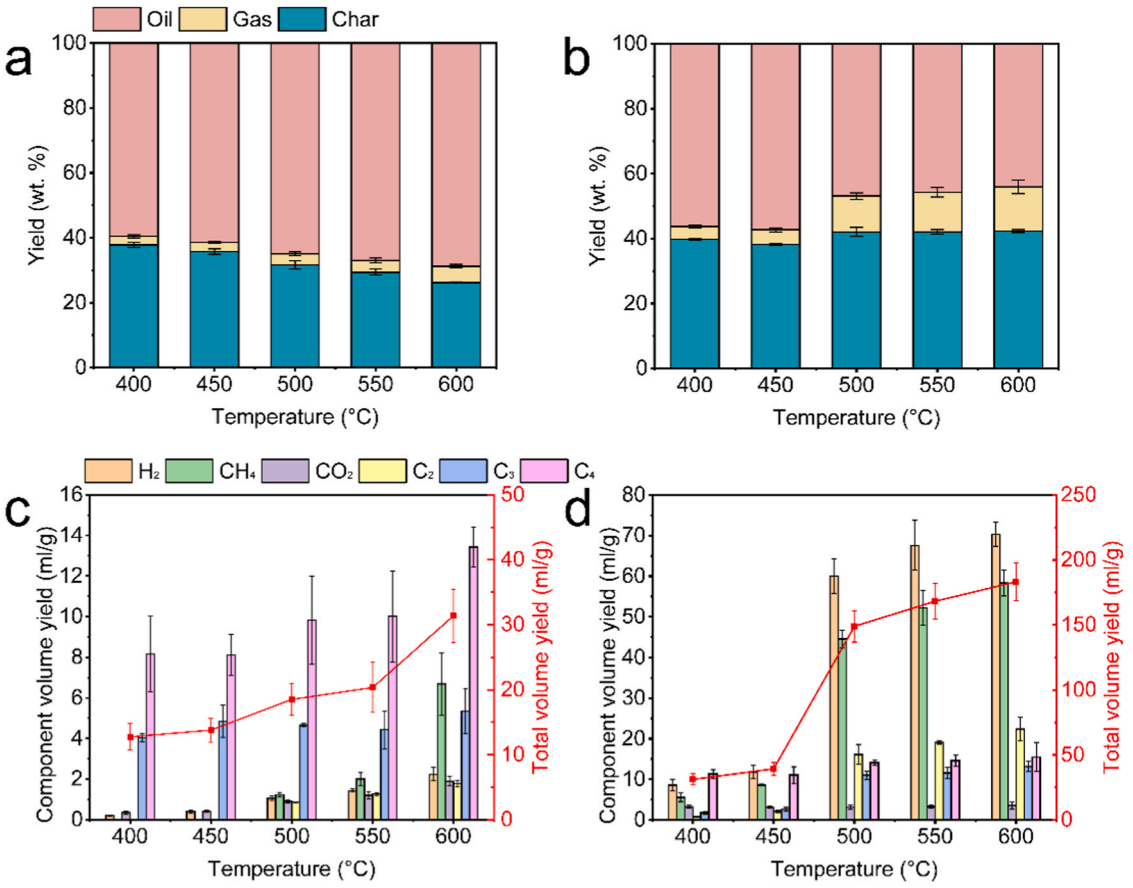

Fig. 4. Product distribution and gas products analysis for fast and slow pyrolysis. The product distributions of a fast and b slow WT pyrolysis. The gas compositions of **c** fast and **d** slow pyrolysis gases.

different final temperatures from both slow and fast pyrolysis are presented in Fig. 4a-b. The char yield did not vary too much at different temperatures for slow pyrolysis of WTs. During slow pyrolysis, the production of gaseous products increased progressively at higher temperatures due to enhanced cracking. As a result, the yield of liquid products decreased because of the further cracking of the liquid into gaseous products.

The product distributions varied a lot with the significant increase in the heating rate. The char yield reduced from 37.81% at 400 °C to 26.21% at 600 °C. The drastic increment in the heating rate led to a higher decomposition of the main organic components. Thus, the difference between the pressure inside and outside a WT particle during the fast pyrolysis resulted in an abrupt release of volatiles within an extremely short period[14]. Due to the short residence time of volatiles inside the particle, fewer secondary gas-solid interactions occurred, which caused more volatiles to be released. Also, the short residence time of volatiles caused fewer secondary cracking reactions which indicated more volatiles were remained as oil/liquid. As discussed above, the kinetic model was changed from D_2 to A_2 which indicated diffusion was no longer a limiting step. There were enough diffusion channels in the solid residual for the volatiles to be released rather than trapped or re-condensed. Therefore, the change in the reaction model could explain the lower char yield and higher volatiles yield observed during the pyrolysis process.

Fig. 4c-d display the yields of main gas components from WTs slow and fast pyrolysis. With an increased temperature from 400° to 600°C, the total gas yields increased from 12.75 to 31.35 ml g^{-1} for fast pyrolysis and 31.19–183.22 ml g^{-1} for slow pyrolysis. Meanwhile, compared with the gas yields of all pyrolysis experiments at the same final temperature but different heating rates, the yield of gaseous products in fast pyrolysis was much lower than that in slow pyrolysis. The WTs fast pyrolysis inhibited volatile dehydrogenation reactions (e.g., aromatization and cyclization reaction), thus generating less H_2 and CH_4. A previous study reported that with the increase of aromaticity in tar, H_2 gradually became a major product because of the volatile secondary reaction[28]. A higher heating rate led to less generation of CH_4 due to less time for volatile cracking[29]. At the same time, less volatile residence time caused C_3∼C_4 to become the main gaseous components in fast pyrolysis.

Fig. 5a-b illustrate the distribution of aliphatic and aromatic compounds from WTs slow and fast pyrolysis. In the fast pyrolysis, the contents of aliphatic and aromatic compounds were constant at ∼90.5% and ∼7.5%, respectively at elevated temperatures. As discussed before, the sharp increase in heating rates could inhibit the secondary reaction of volatiles. The nearly constant distribution of aliphatic and aromatic compounds demonstrated that the oil obtained from the fast pyrolysis was mainly primary pyrolytic fragments. However, in the slow pyrolysis, with the increase in final temperature, the aliphatic compound compositions decreased from 77.79% to 30.38%, but the aromatic compounds increased from 20.16% to 68.64%. The low heating rate and long residence time led to the severe aromatization reaction under the synergistic effect of high temperature. That could be the main reason resulting in the gradual increase in aromatic compound compositions. Moreover, the product distribution also implied that the property of oil generated at the high heating rate could well represent the structure and composition of the primary volatiles.

C_{10}, C_{15}, and C_{15+} aliphatic hydrocarbon compounds were the main components in the aliphatic compounds in both fast and slow pyrolysis. As observed in Fig. 5d-e, the contents of C_{15+} aliphatic hydrocarbons in the fast pyrolysis were higher than those in the slow pyrolysis at all temperatures. C_{15+} compounds were mainly derived from the primary cracking of bonds in the solid phase. Compared with slow pyrolysis, the increase in heavy carbonaceous substances (C_{15+}) indicated that a high heating rate promoted bond rupture in the macromolecular network to generate more heavy components. Furthermore, the reduced residence time resulted in minimal secondary cracking of C_{15+} compounds, leading to their conversion to smaller molecules. The higher contents of C_{10} aliphatic hydrocarbons in the fast pyrolysis indicated that the high heating rate facilitated the cleavage of NR and inhibited the occurrence of further cleavage reaction due to the shorter residence time. Also, a dramatic difference in the contents of C_{15} aliphatic hydrocarbon ($C_{15}H_{24}$) could be discovered in the fast pyrolysis, which indicated high heating rates favored the formation of trimers of isoprene (Fig. 5f). The difference also indicated the change of chemical bond breakage progress with the increase in heating rate during the WTs pyrolysis, which would be further investigated by density functional theory (DFT) method in the section of DFT calculations.

In order to determine the composition of primary pyrolytic volatiles in the slow pyrolysis, in-situ Py-EI/VUVPI-TOF-MS was employed (Fig. 5c). In Py-EI/VUVPI-TOF-MS system, unlike other in-situ detection systems (TG-MS, TG-GC/MS), the distance between the pyrolysis region and the ionization region was only 2 cm, and the whole system was operated in a high vacuum environment (∼10^{-5} Pa). The above two designs enhanced the mean free path of primary volatiles to inhibit the secondary reactions. Moreover, an EI source (70 eV) to ionize organic matter with low ionization energy was employed in the system to solve the identification difficulties resulting from fragment ions. This system used a VUVPI source (10.6 eV) to effectively eliminate fragment ions by near-threshold ionization. Thus, this novel method could minimize the fragmentation and identify most primary pyrolytic volatiles[30,31]. The gases mainly consisted of water ($m/z = 18$), C_2H_4/CO ($m/z = 28$), H_2S ($m/z = 34$), C_4H_6 ($m/z = 54$) and C_4H_8 ($m/z = 56$). Importantly, the analysis revealed minimal detection of H_2 and CH_4 which demonstrated they were mainly generated from the volatile secondary reactions (e.g., cleavage, aromatization, etc.). Other organic primary volatiles were identified i.e., C_5H_8 ($m/z = 54$), C_7H_{12} ($m/z = 96$), C_8H_{13}·($m/z = 109$), C_9H_{14} ($m/z = 122$), $C_{10}H_{16}$ ($m/z = 136$) and $C_{15}H_{24}$ ($m/z = 204$). Herein, isoprene, C_5H_8 was the monomer of NR, while $C_{10}H_{16}$ and $C_{15}H_{24}$ were the dimer and trimer, respectively. The integration of isoprene and ethylene generated C_7H_{12}. C_9H_{14} was formed by the combination of isoprene and butadiene. Isoprene and propene radicals formed C_8H_{13}·. Since isoprene was the monomer of NR and involved in the formation of many pyrolysis products as shown in Fig. 5c, a DFT study was carried out in the section of DFT calculations to demonstrate the evolvement of NR, monomer, dimer, and trimer of C_5H_8.

3.4. Analysis of WTs fast and slow pyrolytic char

To provide a comprehensive understanding of the WTs pyrolysis kinetics, the analysis of solid products is essential. The results of the ultimate analysis are listed in Table S3. In general, C content increased from 77.55% to 80.72% in the slow pyrolysis at elevated temperatures. However, a totally different variation trend was observed that C content was reduced from 75.26% to 71.88% in the fast pyrolysis. Besides, the values of C/H ratio in fast pyrolysis were lower than those in slow pyrolysis except for 400 °C. The lower C/H ratio observed in the slow pyrolysis process suggested that more unsaturated heavy carbonaceous materials were likely left in the solid product, due to an increased occurrence of secondary gas-solid reactions prior to volatile release from the solid phase. Moreover, 400 °C was too low to fully decompose the WTs. The quicker completion of fast pyrolysis resulted in a lower H content than that in slow pyrolysis because the completed decomposition in fast pyrolysis led to relatively more intensive dehydrogenation.

The evolution of the pore structure of char is depicted in Fig. 6a-b via the N_2 adsorption-desorption method. At the same pyrolysis temperature of 600 °C, the specific surface area gradually increased from 54 to 115 $m^2 g^{-1}$ with an increase in the heating rate from 0.17° to 230°C s^{-1}. The explosive release of volatiles caused a quick increment of pressure inside WT particles, leading to much less residence time of volatiles in the solid phase, which reduced the chances of the recombination reactions for char generation[32]. Thus, more volatiles were generated, leading to a higher surface area and total pore volume. Moreover, the

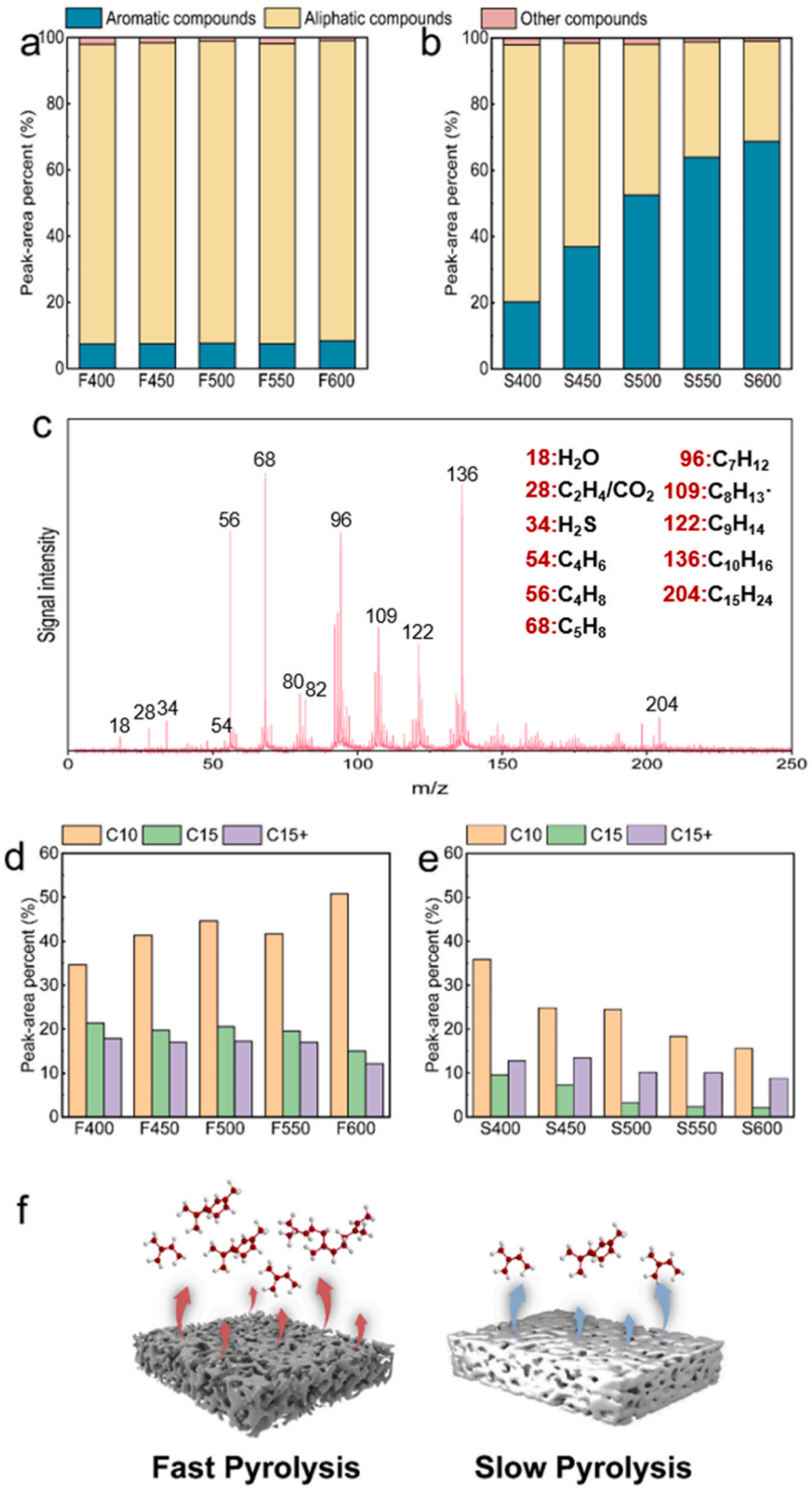

Fig. 5. Liquid products analysis for fast and slow pyrolysis. The aliphatic and aromatic distributions in oil products of a fast and b slow pyrolysis. c EI-MS and VUVPI-MS spectra of primary volatiles from WT slow pyrolysis (Condition: room temperature to 600 °C at a heating rate of 10 °C min^{-1}). The distribution of C_{10}, C_{15}, and C_{15+} aliphatic hydrocarbon compounds of d fast and e slow pyrolysis based on the GC/MS analysis. f The schematic diagram of comparison of fast and slow pyrolysis.

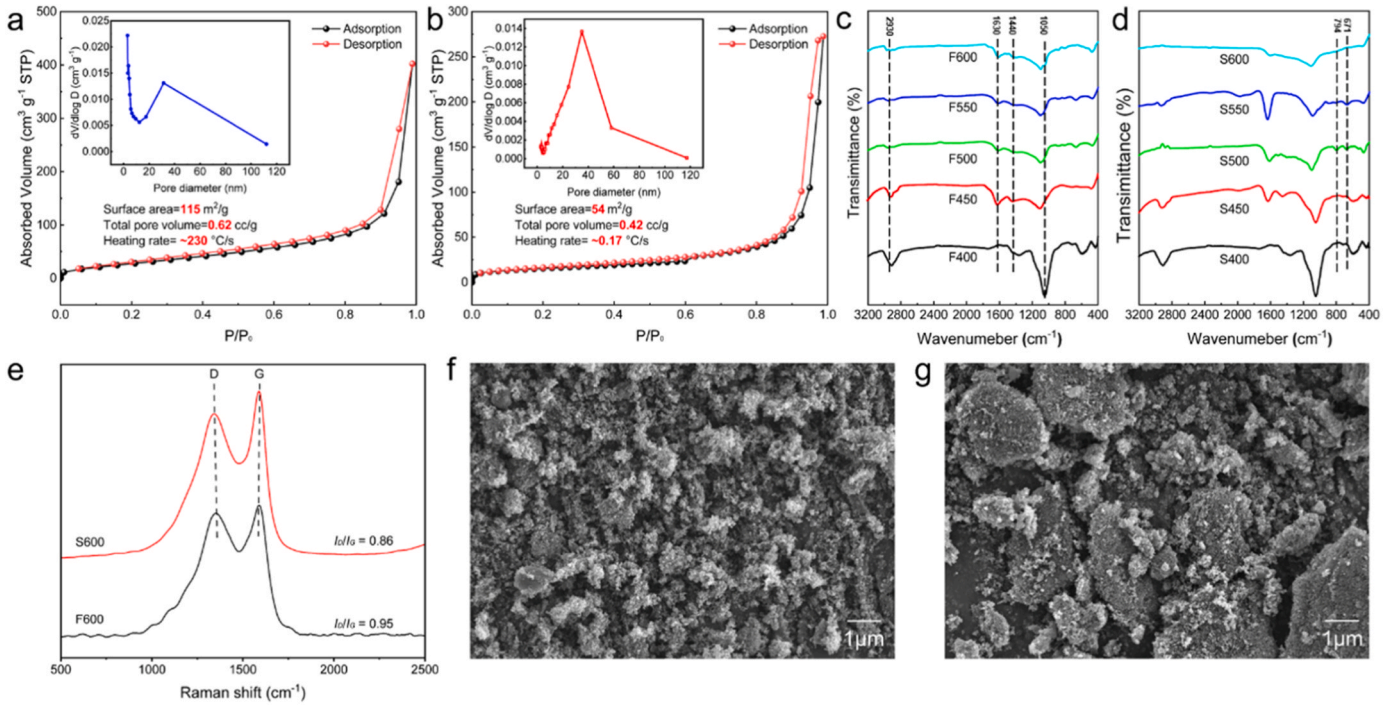

Fig. 6. Pyrolytic char characteristics in the fast and slow pyrolysis. The N_2 adsorption-desorption isotherms and pore size distributions of a fast and b slow pyrolytic char at 600 °C. The FTIR spectra of c fast and d slow pyrolytic char. e The Raman spectra of fast and slow pyrolytic char at 600 °C. The SEM micrographs of **f** fast and **g** slow pyrolytic char at 600 °C.

porous structure facilitated the diffusion of volatiles, which also proved that diffusion was no longer the limitation step in the discussion of kinetics.

The functional group information of the pyrolytic char (fast pyrolysis) surface is depicted in Fig. 6c. The functional groups at 2930 cm^{-1} and 1440 cm^{-1} were caused by the asymmetric bending and stretching vibration corresponding to the C-H from -CH_2- and -CH_3. As the temperature rose, the intensity decreased gradually, indicating dehydrogenation reactions had occurred. The characteristic peaks at 1630, 794, and 671 cm^{-1} were clearly identified as the functional groups (C═C and C-H) of the aromatic compounds. In the slow pyrolysis, these peaks could also be identified. Nevertheless, compared with fast pyrolysis, the intensity increased evidently, indicating low heating rates favored the formation of unsaturated aromatics, and high heating rates enhanced the dehydrogenation.

In order to demonstrate the change of reaction mechanism from F_{2-3} to A_2 arose from the increase in heating rate, the Raman test was carried out (Fig. 6e). Generally, the D band represented the defects and disorder in the carbon layers[33]. The G band represented the graphitization degree of carbon structure, which was caused by the in-plane stretching vibration of sp^2 hybridization[34]. The defective degree of the carbon materials could be reflected by the intensity ratio of the D band over the G band (I_D/I_G) [35]. The values were 0.95 (F600) and 0.86 (S600). The increased I_D/I_G values implied more defective sites were generated for the char produced at 600 °C through fast pyrolysis to facilitate the nucleation and nuclei growth[36].

The microscopic morphologies of F600 and S600 are depicted in Fig. 6f-g. The rougher surface of F600 could provide more nuclei to facilitate the occurrence of nucleation and nuclei growth.

3.5. DFT calculations of WTs pyrolysis processes

For an in-depth understanding of WTs fast and slow pyrolysis processes, a DFT analysis was carried out. The degradation mechanism was discovered at the m06–2x/6–311 g(d,f) level by using the Gaussian16 software package[37]. Intrinsic reaction coordinate (IRC) analysis was also performed to verify the obtained transition state that linked the designated reactants and products. According to the characteristics of kinetics and products, the thermal degradation of polyisoprene was dominant in the pyrolysis processes. Thus, the difference in the cracking mechanism of polyisoprene between the two distinct thermal histories was important. Moreover, $C_{15}H_{24}$ (trimer) was the biggest unit of isoprene which had been identified by the Py-EI/VUVPI-TOF-MS. Thus, trimer, dimer, and monomer of isoprene could be released as volatiles through the decomposition of the solid WTs samples, but tetramer or larger polymer could not be released in terms of volatiles. Furthermore, it was assumed that the thermal degradation of all polymers followed the random bond-breaking principle.

In the case of dimer breaking into two monomers as shown in Fig. 7 (DP=2), the energy barrier was noticeably higher indicating it was more difficult to produce monomers from dimer than from larger polymers (DP>2). When DP> 2, there were many different possibilities to break the polymer. In the case of DP= 3, the random bond scission could form a monomer and a dimer; in the case of DP= 4, the cleavage had two possibilities, forming a monomer and a trimer, or forming two monomers. The black, red, blue, and green curves were corresponding to the pathways to form monomers, dimers, trimers, and tetramers (A more graphical explanation of the pathways and the structures of the transition states are depicted in Fig. S6-S7). It was obvious that for DP> 2, the uneven breakage forming a monomer together with a larger polymer (DP= *n*-1) was easier to occur due to the lower energy barrier. Rupture at more central positions was less likely owing to the higher free energy. When WTs were heated slowly, only low-energy-barrier reactions could occur. This implied the monomers were ruptured off one by one. However, the degradation reaction had already been in a high-temperature environment (Fig. S8) due to the rapid heating rate for fast pyrolysis, which increased the possibility of triggering high-energy-barrier reactions. During fast pyrolysis, more bond locations were available to break compared with slow pyrolysis, and the total degradation rate was higher than that in slow pyrolysis. The multi-isoprene polymer units could continue the cleavage reaction under the same mechanism until the polymerization of units was less than or equal to three. Thus, in WTs

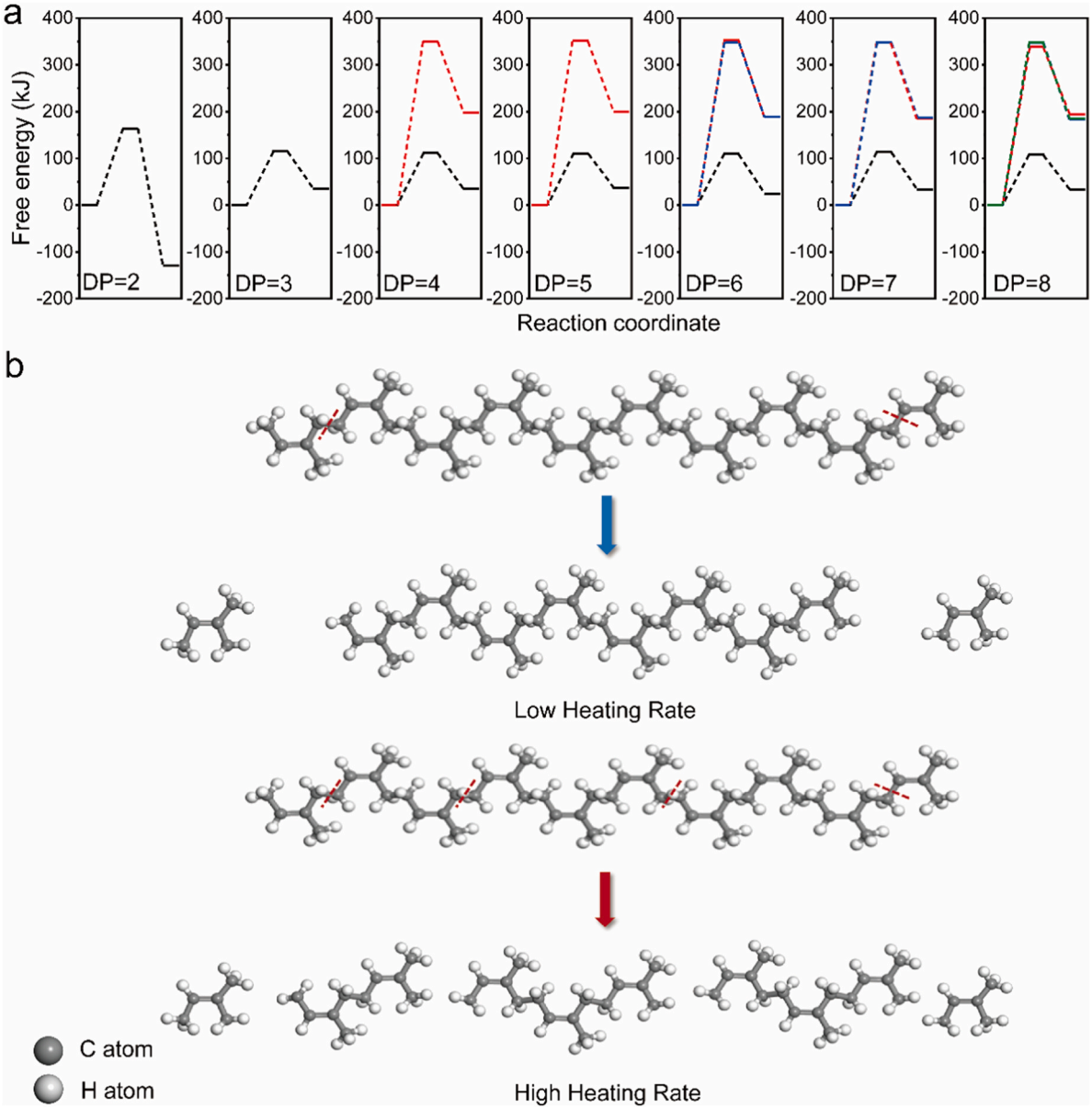

Fig. 7. Free-energy diagrams of the pyrolysis processes. a The polymer with different degrees of polymerization. The cleaved units were monomer (black line), dimer (red line), trimer (blue line) and tetramer (green line), respectively. b The schematic diagram for the polyisoprene scission.

fast pyrolysis, the content of isoprene trimer was higher than that in the slow pyrolysis as observed in Fig. 5d-e. Two different cracking processes of the rubber polymer were discovered through the DFT analysis.

As mentioned above, higher heating rate and pressure difference caused fewer occurrences of cracking reactions, leading to less cleavage of trimer into monomer/dimer. The apparent activation energy has no practical physical meaning in the microscopic sense, and it is the algebraic sum of activation energies of each elementary reaction. Since there were more occurrences of the elementary reaction in the slow pyrolysis process, it exhibited higher apparent activation energy. Moreover, the volatile release could be expressed as sample weight loss at a macroscopic perspective. The rapid release of the volatiles and fewer cracking reactions in the fast pyrolysis process were responsible for the significant increase in the degradation rate. Overall, both experimental observations and theoretical calculations indicated that WTs fast pyrolysis tended to produce more isoprene trimers.

4. Conclusion

To investigate the fast pyrolysis kinetics and product distributions of waste tires (WTs), a novel thermo-balance device was developed. The results revealed that increasing the heating rate had a significant impact on the pyrolysis kinetics and product yields. The accelerated heating process led to a substantial portion of WTs pyrolysis taking place during the isothermal stage, which increased the formation of trimer isoprene and led to a decrease in the apparent activation energy. Moreover, the change of the reaction model from F_{2-3} to A_2 was supported by the discovery that more detects and rougher surfaces were formed on the pyrolytic char due to the significant increment of the reaction rate. From the perspective of pyrolytic products, high heating rates led to a rapid thermal decomposition so that more volatiles and interspace were generated. Hence, secondary polymerization and cracking reactions were inhibited. Even at 600 °C, there was still a considerable yield of pyrolytic oil which surpassed conventional wisdom that rising temperature favored the cracking reaction of oil into gas. Isoprene and its

polymers were identified as the primary pyrolytic volatiles of WTs, and density functional theory calculations confirmed that trimer isoprene formation was easier during fast pyrolysis. Additionally, the significant pressure difference between the inside and outside of the WTs particles led to faster release of volatiles, reducing the potential for trimer cracking into monomer or dimer in the solid phase, which favored the release of trimer isoprene and ultimately contributed to the change in the WTs pyrolysis reaction mechanism. These findings offered valuable insights for the development of WTs and other organic waste pyrolysis technologies in the industry.

Environmental Implication

Fast pyrolysis has emerged as an effective method in reducing the environmental risks associated with waste tires. However, the limitations of heating rates in commercial thermogravimetric analyzers (TGA) have hindered the analysis of fast pyrolysis behavior in industrial reactors. In this study, we propose an approach to investigate the fast pyrolysis kinetics and product-formation mechanisms during waste tire pyrolysis under extremely high heating rates. Our novel approach provides a new perspective for the development of waste tire pyrolysis technologies and represents a significant contribution to the field.

CRediT authorship contribution statement

B.Q., C.L. and Y.W. conceived the experimental investigation. B.Q., C.L. and Y.W. performed the measurements and analyzed the data. B.Q., C.L. and Y.W. contributed conceptualization. G.J., A.L. and Y.S.Z contributed methodology; B.Q. contributed to the original draft preparation. G.J, A.L. and Y.S.Z contributed project supervision, G.J. and A.L. contributed funding acquisition. All authors have read and agreed to the submitted version of the manuscript.

Declaration of Competing Interest

The authors declare that they have no known competing financial interests or personal relationships that could have appeared to influence the work reported in this paper.

Data Availability

Data will be made available on request.

Acknowledgements

Authors appreciate the financial support from the Liao Ning Revitalization Talents Program (grant number: XLYC2007179).

Author Contributions

The manuscript was written through contributions of all authors. All authors have approved the final version of the manuscript.

Appendix A. Supporting information

Supplementary data associated with this article can be found in the online version at doi:10.1016/j.jhazmat.2023.132494.

References

[1] Thomas, B.S., Gupta, R.C., 2016. A comprehensive review on the applications of waste tires rubber in cement concrete. Renew Sustain Energy Rev 54, 1323–1333.
[2] Ul Islam, M.M., Li, J., Roychand, R., Saberian, M., Chen, F., 2022. A comprehensive review on the application of renewable waste tires rubbers and fibers in sustainable concrete. J Clean Prod 374, 133998.
[3] Tian, Z., Zhao, H., Peter, K.T., Gonzalez, M., Wetzel, J., Wu, C., Hu, X., Prat, J., Mudrock, E., Hettinger, R., Cortina, A.E., Biswas, R.G., Kock, F.V.C., Soong, R., Jenne, A., Du, B., Hou, F., He, H., Lundeen, R., Gilbreath, A., Sutton, R., Scholz, N. L., Davis, J.W., Dodd, M.C., Simpson, A., McIntyre, J.K., Kolodziej, E.P., 2021. A ubiquitous tires rubber–derived chemical induces acute mortality in coho salmon. Science 371, 185–189.
[4] Trang, B., Li, Y., Xue, X.-S., Ateia, M., Houk, K.N., Dichtel, W.R., 2022. Low-temperature mineralization of perfluorocarboxylic acids. Science 377, 839–845.
[5] Sikarwar, V.S., Zhao, M., Clough, P., Yao, J., Zhong, X., Memon, M.Z., Shah, N., Anthony, E.J., Fennell, P.S., 2016. An overview of advances in biomass gasification. Energy Environ Sci 9, 2939–2977.
[6] Ding, Z., Chen, Z., Liu, J., Evrendilek, F., He, Y., Xie, W., 2022. Co-combustion, life-cycle circularity, and artificial intelligence-based multi-objective optimization of two plastics and textile dyeing sludge. J Hazard Mater 426, 128069.
[7] Wu, L., Xin, J., Xia, D., Sun, J., Liang, J., 2022. Enhanced production of hydrocarbons from the catalytic pyrolysis of maize straw over hierarchical ZSM-11 zeolites. Appl Catal B: Environ 317, 121775.
[8] Ding, Z., Chen, H., Liu, J., Cai, H., Evrendilek, F., Buyukada, M., 2021. Pyrolysis dynamics of two medical plastic wastes: drivers, behaviors, evolved gases, reaction mechanisms, and pathways. J Hazard Mater 402, 123472.
[9] Tang, X., Chen, X., He, Y., Evrendilek, F., Chen, Z., Liu, J., 2022. Co-pyrolytic performances, mechanisms, gases, oils, and chars of textile dyeing sludge and waste shared bike tires under varying conditions. Chem Eng J 428, 131053.
[10] Jie, X., Li, W., Slocombe, D., Gao, Y., Banerjee, I., Gonzalez-Cortes, S., Yao, B., AlMegren, H., Alshihri, S., Dilworth, J., Thomas, J., Xiao, T., Edwards, P., 2020. Microwave-initiated catalytic deconstruction of plastic waste into hydrogen and high-value carbons. Nat. Catal. 3, 902–912.
[11] Regalbuto, J.R., 2009. Cellulosic biofuels—got gasoline? Science 325, 822–824.
[12] Zhang, S., Jiang, S.-F., Huang, B.-C., Shen, X.-C., Chen, W.-J., Zhou, T.-P., Cheng, H.-Y., Cheng, B.-H., Wu, C.-Z., Li, W.-W., Jiang, H., Yu, H.-Q., 2020. Sustainable production of value-added carbon nanomaterials from biomass pyrolysis, Nature. Sustainability 3, 753–760.
[13] Liu, W.-J., Jiang, H., Yu, H.-Q., 2019. Emerging applications of biochar-based materials for energy storage and conversion. Energy Environ Sci 12, 1751–1779.
[14] Xu, S., Zeng, X., Han, Z., Cheng, J., Wu, R., Chen, Z., Masěk, O., Fan, X., Xu, G., 2019. Quick pyrolysis of a massive coal sample via rapid infrared heating. Appl Energy 242, 732–740.
[15] Li, T., Song, F., Wu, F., Huang, X., Bai, Y., 2022. Heterogeneous dynamic behavior and synergetic evolution mechanism of internal components and released gases during the pyrolysis of aquatic biomass. Environ Sci Technol 56, 13595–13606.
[16] Kumar, A., Yan, B., Tao, J., Li, J., Kumari, L., Tafa Oba, B., Akintayo Aborisade, M., Ali Jamro, I., Chen, G., 2022. Co-pyrolysis of de-oiled microalgal biomass residue and waste tires: Deeper insights from thermal kinetics, behaviors, drivers, bio-oils, bio-chars, and in-situ evolved gases analyses. Chem Eng J 446, 137160.
[17] Tang, X., Chen, Z., Liu, J., Chen, Z., Xie, W., Evrendilek, F., Buyukada, M., 2021. Dynamic pyrolysis behaviors, products, and mechanisms of waste rubber and polyurethane bicycle tires. J Hazard Mater 402, 123516.
[18] Zhang, Y., Niu, Y., Zou, H., Lei, Y., Zheng, J., Zhuang, H., Hui, S., 2017. Characteristics of biomass fast pyrolysis in a wire-mesh reactor. Fuel 200, 225–235.
[19] Qu, B., Li, A., Qu, Y., Wang, T., Zhang, Y., Wang, X., Gao, Y., Fu, W., Ji, G., 2020. Kinetic analysis of waste tires pyrolysis with metal oxide and zeolitic catalysts. J Anal Appl Pyrolysis 152, 104949.
[20] Vyazovkin, S., Burnham, A.K., Criado, J.M., Pérez-Maqueda, L.A., Popescu, C., Sbirrazzuoli, N., 2011. ICTAC kinetics committee recommendations for performing kinetic computations on thermal analysis data. Thermochim Acta 520, 1–19.
[21] Criado, J.M., Pérez-Maqueda, L.A., 2005. Sample controlled thermal analysis and kinetics. J Therm Anal Calorim 80, 27–33.
[22] Mkhize, N.M., Danon, B., van der Gryp, P., Görgens, J.F., 2019. Kinetic study of the effect of the heating rate on the waste tyre pyrolysis to maximise limonene production. Chem Eng Res Des 152, 363–371.
[23] Sun, D., Kandare, E., Maniam, S., Zhou, A., Robert, D., Buddhacosa, N., Giustozzi, F., 2022. Thermal-based experimental method and kinetic model for predicting the composition of crumb rubber derived from end-of-life vehicle tyres. J Clean Prod 357, 132002.
[24] Seidelt, S., Müller-Hagedorn, M., Bockhorn, H., 2006. Description of tires pyrolysis by thermal degradation behaviour of main components. J Anal Appl Pyrolysis 75, 11–18.
[25] Koga, N., Vyazovkin, S., Burnham, A.K., Favergeon, L., Muravyev, N.V., Pérez-Maqueda, L.A., Saggese, C., Sánchez-Jiménez, P.E., 2023. ICTAC Kinetics Committee recommendations for analysis of thermal decomposition kinetics. Thermochim Acta 719, 179384.
[26] Zhang, Y., Wu, C., Nahil, M.A., Williams, P., 2016. High-value resource recovery products from waste tyres. Proc Inst Civ Eng - Waste Resour Manag 169, 137–145.
[27] Khawam, A., Flanagan, D.R., 2006. Solid-state kinetic models: basics and mathematical fundamentals. J Phys Chem B 110, 17315–17328.
[28] Chen, Z., Wang, D., Li, C., Yang, H., Wang, D., Lai, D., Yu, J., Gao, S., 2020. A tandem pyrolysis-upgrading strategy in an integrated reactor to improve the quality of coal tar. Energy Convers Manag 220, 113065.
[29] Zaini, I.N., Gomez-Rueda, Y., García López, C., Ratnasari, D.K., Helsen, L., Pretz, T., Jönsson, P.G., Yang, W., 2020. Production of H2-rich syngas from excavated landfill waste through steam co-gasification with biochar. Energy 207, 118208.
[30] Yang, J., Wu, Y., Zhu, J., Yang, H., Li, Y., Jin, L., Hu, H., 2023. Insight into the pyrolysis behavior of polyvinyl chloride using in situ pyrolysis time-of-flight mass spectrometry: aromatization mechanism and Cl evolution. Fuel 331, 125994.
[31] Zhu, J., Xu, J., Hu, H., Wang, X., Zhou, Y., Jin, L., 2021. Novel detection of primary and secondary volatiles from cedar pyrolysis using in-situ pyrolysis double ionization time-of-flight mass spectrometry. Chem Eng Sci 236, 116545.

[32] Gray, V.R., 1988. The role of explosive ejection in the pyrolysis of coal. Fuel 67, 1298–1304.
[33] Cai, S., Zhang, Q., Wang, Z., Hua, S., Ding, D., Cai, T., Zhang, R., 2021. Pyrrolic N-rich biochar without exogenous nitrogen doping as a functional material for bisphenol A removal: performance and mechanism. Appl Catal B: Environ 291, 120093.
[34] Liang, L., Wang, Y., Li, N., Yan, B., Chen, G., Hou, La, 2022. Breaking rate-limiting steps in a red mud-sewage sludge carbon catalyst activated peroxymonosulfate system: effect of pyrolysis temperature. Sep Purif Technol 299, 121805.
[35] Ni, J., Gao, Y., Sun, Y., Ji, G., Li, A., 2022. High-efficiency removal of antibiotic pollutants by magnetic carbon aerogel: Inherent roles of adsorption synergistic catalysis. J Clean Prod 375, 134105.
[36] Qu, Y., Li, A., Wang, D., Zhang, L., Ji, G., 2019. Kinetic study of the effect of in-situ mineral solids on pyrolysis process of oil sludge. Chem Eng J 374, 338–346.
[37] Frisch, M.J., Trucks, G.W., Schlegel, H.B., Scuseria, G.E., Robb, M.A., Cheeseman, J.R., Scalmani, G., Barone, V., Petersson, G.A., Nakatsuji, H., Li, X., Caricato, M., Marenich, A.V., Bloino, J., Janesko, B.G., Gomperts, R., Mennucci, B., Hratchian, H.P., Ortiz, J.V., Izmaylov, A.F., Sonnenberg, J.L., Williams, F., Ding, F., Lipparini, F., Egidi, J., Goings, B., Peng, A., Petrone, T., Henderson, D., Ranasinghe, V.G., Zakrzewski, J., Gao, N., Rega, G., Zheng, W., Liang, M., Hada, M., Ehara, K., Toyota, R., Fukuda, J., Hasegawa, M., Ishida, T., Nakajima, Y., Honda, O., Kitao, H., Nakai, T., Vreven, K., Throssell, J.A., Montgomery Jr, J.E., Peralta, F., Ogliaro, M.J., Bearpark, J.J., Heyd, E.N., Brothers, K.N., Kudin, V.N., Staroverov, T.A., Keith, R., Kobayashi, J., Normand, K., Raghavachari, A.P., Rendell, J.C., Burant, S.S., Iyengar, J., Tomasi, M., Cossi, J.M., Millam, M., Klene, C., Adamo, R., Cammi, J.W., Ochterski, R.L., Martin, K., Morokuma, O., Farkas, J.B., Foresman, D.J., Fox, 2016. A.03, in, Wallingford, CT, 16 Rev..,. Gaussian,.